Review: Active Control of Shock-associated Unsteady Flow Phenomena in Aeroengines

- Suppression Techniques for Transonic Cascade Flutter and Supersonic Jet Noise -

Toshinori Watanabe
Department of Aeronautics and Astronautics
The University of Tokyo
Tokyo, Japan
watanabe@aero.t.u-tokyo.ac.jp

Abstract

Active control techniques for cascade flutter suppression and supersonic jet noise reduction were studied in the University of Tokyo. For flutter suppression, piezoelectric devices were installed on the blade surfaces. The active oscillation of the trailing edge of a blade was found to suppress the flutter instability in the numerical analysis. The effect was qualitatively confirmed in a trial experiment. For jet noise reduction, the technique of microjet injection was experimentally studied. The microjet could provide quite effective reduction of shock associated noise through the suppression of jet oscillation. The present paper briefly introduces these studies.

1. Introduction

Active control of unsteady flow is thought to be one of the key issues for future environmentally-friendly aeroengines with ultra-high reliability and efficiency. Recently, the active suppression techniques of transonic cascade flutter and supersonic jet noise were proposed and studied in the University of Tokyo.

For suppression of cascade flutter, a control method with active oscillation on the blade trailing edge was proposed, and feasibility study was performed with a developed numerical method with flow-structure coupling under transonic flow condition [(1)]. The active oscillation of the trailing edge was realized by use of piezoelectric device [(2)]. From the numerical results, the control method was confirmed effective if the phase difference between the original blade vibration and the active trailing edge oscillation was adequately selected. A trial experiment was also performed in a subsonic flow to verify that the active trailing edge oscillation with piezoelectric device could generate effective unsteady aerodynamic force for changing blade vibration stability [(3)]. Since the stable vibration range in the inter blade phase angle was found to be slightly but substantially widened, the control technique seemed promising for future application for flutter suppression.

For suppression of supersonic jet noise, the technique of microjet injection was experimentally examined [(4), (5)]. A high aspect-ratio rectangular nozzle was adopted as the jet nozzle based on the expectation that the combination of non-circular nozzle and microjet injection could be effective for reduction of

supersonic jet noise. The nozzle was equipped with forty-four evenly spaced micro-nozzles at the long sides of the nozzle exit. Far-field acoustic measurements were conducted for widely ranged microjet conditions to understand the influence of the microjet on characteristics of supersonic jet noise as well as the flow field. For understanding the unsteady behavior of jet and shear layer, flow visualization was performed with schlieren technique using a high-speed camera. A remarkable noise reduction was found in the acoustic data, and the dramatic change in the unsteady flow behavior was observed in the flow visualization.

In the present paper, the results of these two studies are reviewed to show the possibility of active control for future aeroengines.

2. Suppression of Cascade Flutter with Piezoelectric Device

2.1 Numerical Analysis

A developed code of flow-structure coupling method was used for the numerical analysis. The unsteady aerodynamic force acted on all blades was calculated in the flow computation based on the 2D Euler equations. The obtained unsteady aerodynamic force was introduced into the structural computation. The structural model of the blade was a simple one of a translational mode. In the structural computation, the equation of motion of the blade was solved with Runge-Kutta-Gill scheme to obtain the blade displacement. The lift force on the blade calculated in the flow computation was introduced into the equation of motion of the blade, and the computed blade displacement was used for generation of new grid coordinates in the following time step of flow computation. The structural damping was neglected for focusing on the aerodynamic damping effect.

The two-dimensional non-linear Euler equations were solved with a second order upwind TVD scheme. The incorporated Euler iteration introduced second order accuracy in time. The inviscid computation was performed based on the knowledge that the dominant factor of the vibration instability was the unsteady aerodynamic force induced by the oscillation of passage shock wave for the adopted cascade model.

The computational domain, numerical grid (H-O-H configuration) and boundary conditions are shown in Fig. 1. At the inlet boundary, the total pressure, the total temperature, and the tangential velocity were fixed. The static pressure was specified at the outlet boundary, and the blade surfaces were treated as slip walls.

The tip section of Quiet Fan B in NASA Quiet Engine Program [6] was adopted as a model cascade. The inlet Mach number was 1.25, and the pressure ratio p_r was 1.7. The passage shock movement was known to be dominant for blade vibration stability in the adopted case [7]. Figure 2 shows the computed steady Mach contour diagram. A passage shock is generated at the trailing edge of each blade, and its oscillation due to blade vibration induces unsteady aerodynamic force on the pressure surface of the neighboring blade.

Figure 3 describes the proposed active control method. Since the vibration

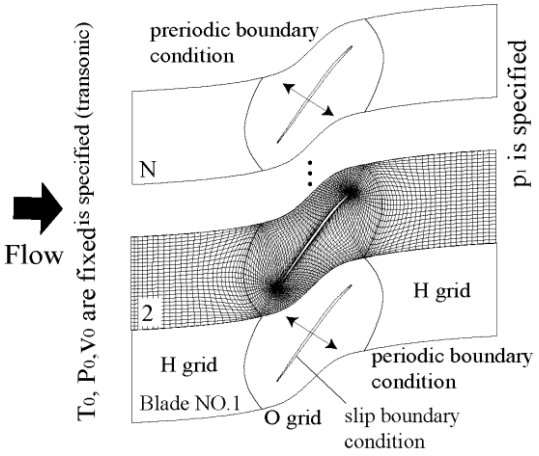

Fig.1 Computational Domain, Grid and Boundary Conditions

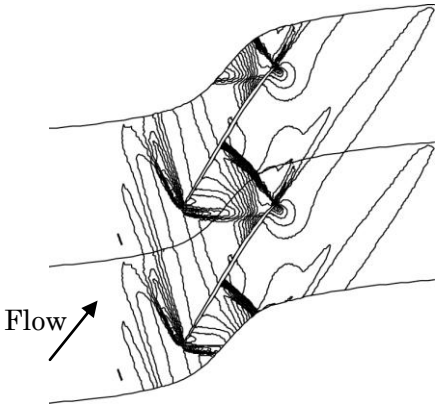

Fig.2 Mach Contour Diagram
(Inlet Mach 1.25, Interval 0.05)

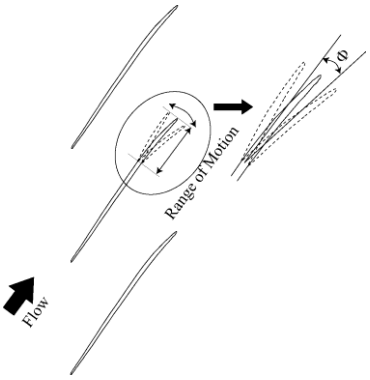

Fig.3 Trailing Edge Oscillation

stability is supposed to be changed by the active control of passage shock movement, the trailing edge of the blade is actively oscillated like a flap. The trailing edge oscillation can be realized by use of piezoelectric devices. The blade vibration due to the shock oscillation and the active trailing edge oscillation by piezoelectric device are separately considered.

Four flow channels were used in the computation to simulate the inter blade phase angle, σ, of 90 degrees, which corresponded to an unstable condition of the cascade flutter. The reduced frequency, *k*, was 0.086 based on the chord length of blade and inlet velocity. All blades were set stationary in the initial situation, and

a sinusoidal disturbance was given to the axial velocity at the inlet boundary during the time t_s, a period of blade natural oscillation.

The activation timing of the control was determined based on the total energy, E, of a blade. The total energy is composed of kinetic energy and elastic energy of a blade. In the time period when E is larger than a specified threshold value, E_0, the trailing edges of blade 1 and blade 3 are actively oscillated. The amplitude of trailing edge oscillation angle was fixed to be 0.5 degrees.

From the results, the control method was found to be effective if the phase difference between trailing edge oscillation and blade vibration, δ, was adequately set. δ is positive when the phase angle of trailing edge oscillation advances that of the blade vibration. The most effective suppression was obtained when δ was +45 degrees. Figure 4 shows time traces of the blade displacement and unsteady aerodynamic force acted on the blade when δ is +45 degrees. Solid lines indicate the results in the case with control and the dotted lines show those in the case without control. The shaded areas in the figures correspond to the periods when the trailing edge oscillation is active. E_0 is determined to be a value of the total energy when the amplitude of blade oscillation is about 0.2% of the chord length. From the comparison between the results of solid and dotted lines, the increase in the blade displacement is seen to be effectively suppressed for both No.1 (controlled) and No.2 (non-controlled) blades by the active control of trailing edge oscillation.

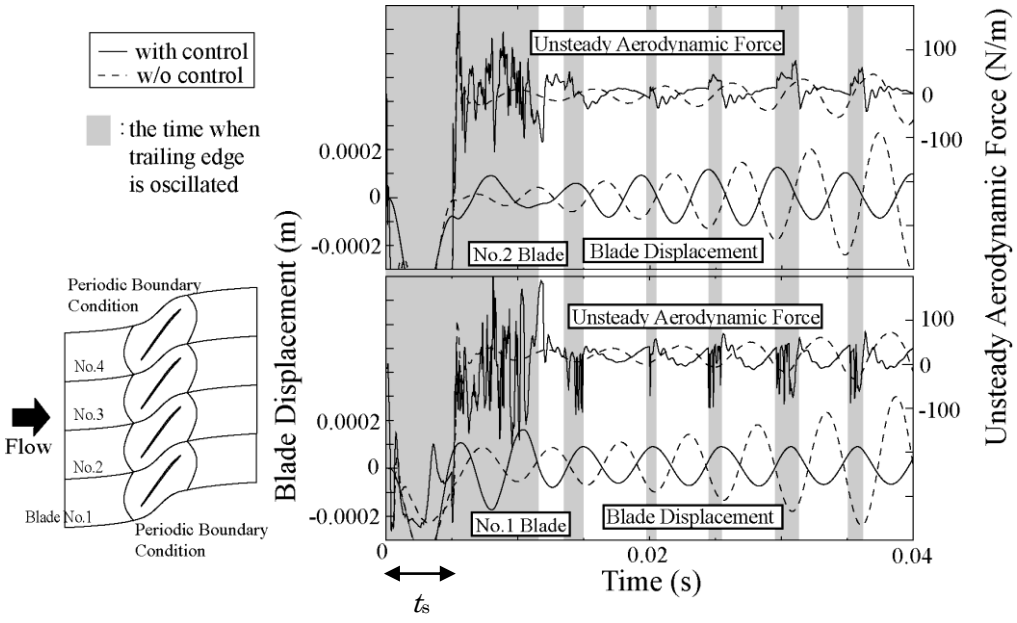

Fig.4 Time History of Blade Displacement and Unsteady Aerodynamic Force

2.2 Experimental Study

The blow-down type linear cascade wind tunnel used in the experiment is schematically shown in Fig. 5. The test section has 50 mm×100 mm rectangular cross section. The test section and the cascade configuration are illustrated in Fig.6. The cascade is composed of 7 Double Circular Arc (DCA) airfoil blades. The inlet Mach number is 1.2 and the incidence angle is 0 degree. The cascade configuration is not the same one as in the numerical study due to the limitation of test facility. The objective of the present experiment is, accordingly, to examine the possibility of active control on unsteady aerodynamic force in a qualitative sense.

An example of steady flow field, visualized by shadow graph method, is shown in Fig. 7. A leading edge oblique shock is clearly seen on each blade, and a passage shock can be seen in blade-to-blade flow channel.

The Influence Coefficient Method was used for analyzing unsteady aerodynamic characteristics of the oscillating blade. The central blade (No.0) was oscillated in a translational mode by a crank mechanism, while the other blades were stationary. The unsteady aerodynamic force induced by the oscillation of No.0 blade was measured with strain gauge system shown in Fig. 8 on No.0 blade, and No. ± 1 blades. The unsteady aerodynamic work coefficient of the blade No. n, $C_{f,n}(\sigma)$, is calculated by the following equation,

$$C_{f,n}(\sigma) = C_n \sin(\delta_a - n\sigma) \qquad (1)$$

where, n is the blade number, C_n is the amplitude of unsteady aerodynamic work on each blade, and δ_a is the phase difference between the blade displacement and the unsteady aerodynamic force. These values are calculated through Fourier decomposition. The unsteady aerodynamic work coefficient of each blade is linearly superposed as Eq. (2) to obtain the unsteady aerodynamic work when all blades are oscillating with an arbitrary inter blade phase angle.

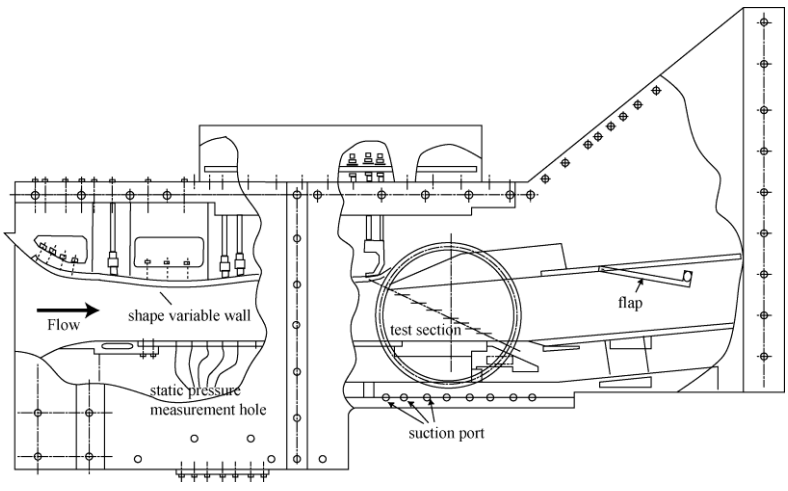

Fig.5 Transonic Linear Cascade Wind Tunnel

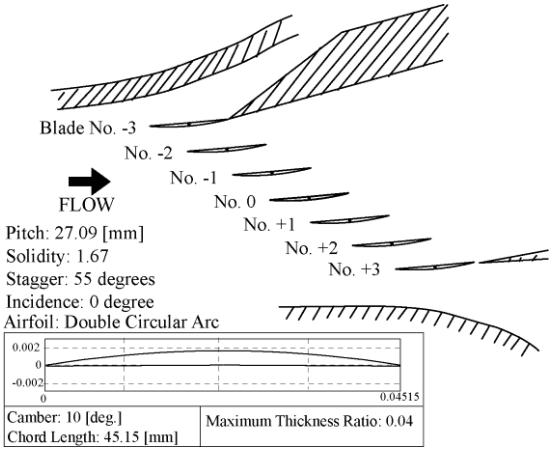

Fig.6 Test Section and Cascade Configuration

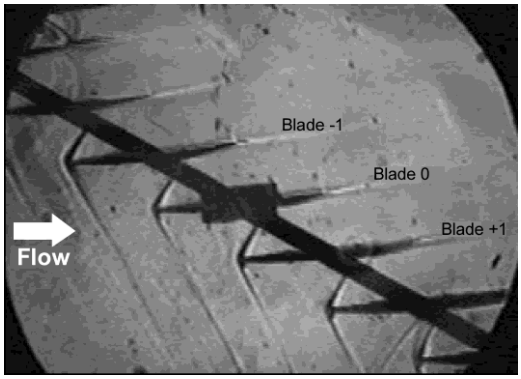

Fig.7 Flow Field around Cascade

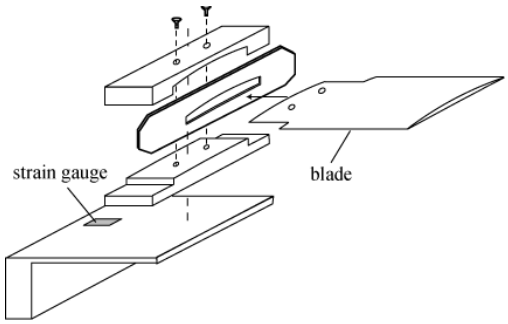

Fig.8 Measuring System for Aerodynamic Force

$$W(\sigma) = \sum_{n=-m}^{m} C_{f,n}(\sigma) \qquad (2)$$

Figure 9 shows the control blade equipped with piezoelectric devices. The two devices were glued on the suction and pressure sides of the blade. The electric signals drove the piezo-oscillation with arbitrary frequency, and the frequency range from 10 to 50 Hz was used in the experiment. Figure 10 shows the amplitude contour of piezo-blade when AC voltage was provided on the device. Amplitude at the tip section is seen to larger than that at the hub section, and the amplitude at trailing edge (T.E.) is larger than that at leading edge (L.E.) over the whole span. Though the oscillation mode was not necessarily correspondent to the numerical model, the blade was used as it was in the present experiment for feasibility study of the control method.

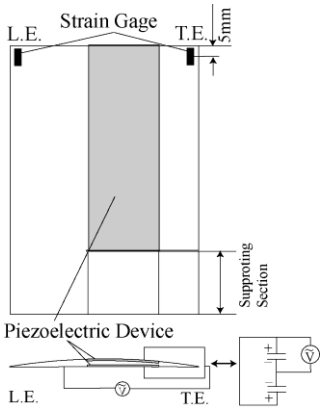

Fig.9 Blade with Piezoelectric Device

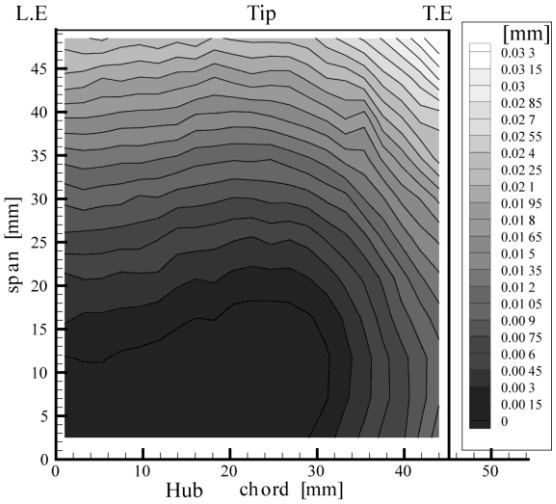

Fig. 10 Amplitude Contour of Piezo-Blade

The piezo-blade was oscillated with the same frequency as that of the translational oscillation of blade No.0 by crank mechanism. From the measured results of unsteady aerodynamic force, the unsteady aerodynamic work at each δ is calculated. The influences of blade vibration and the active oscillation by piezoelectric device are separately considered in the experiment because of the difficulty in simultaneous execution of both oscillations. The unsteady aerodynamic forces were measured separately for the case with blade vibration and for the case with active oscillation by piezoelectric device. The measured data are superposed each other.

The superposed unsteady aerodynamic work is plotted against the inter blade phase angle in Fig. 11 for the case of k=0.018. The result of original case without control is also plotted for comparison. When δ is 120 degrees, the superposed aerodynamic work shows substantial reduction in unstable aerodynamic work in the range of σ where the original blade vibration is unstable. The range of positive work indicating flutter instability is shown to be slightly reduced as well. These results indicate the stabilization effect of the active oscillation of the piezoelectric device. On the contrary, when δ is -60 degrees, the blade vibration is destabilized by the active oscillation.

2.3 Concluding Remarks

From the numerical and experimental results, the active trailing edge oscillation was found to have substantial suppression effect on flutter instability in transonic flow if the phase difference between the blade vibration and the trailing edge oscillation was properly selected. However, the instability could be enhanced due to inappropriate selection of the phase difference. The optimum phase difference should be sensitive to the aerodynamic and structural characteristics of the blades.

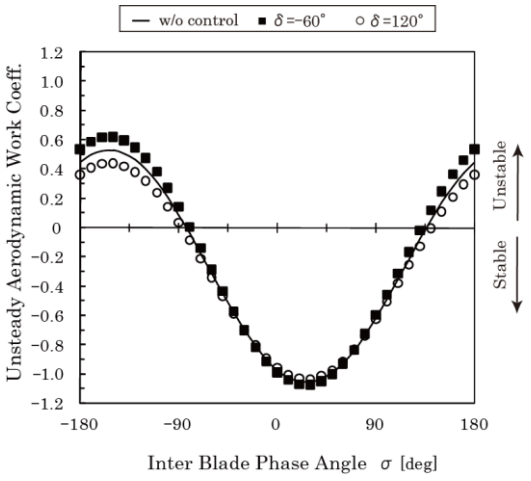

Fig.11 Resultant Unsteady Aerodynamic Work

3. Suppression of Supersonic Jet Noise with Microjet Injection

For environmentally-friendly civil transport, jet noise is a crucial problem. Since jet noise becomes very intense in the case of supersonic aircraft, noise reduction is one of the most important technical issues for the realization of next-generation supersonic transport.

Various kinds of methods for reducing jet noise have been proposed so far, and many researches have been made to clarify their effectiveness and to understand their flow mechanisms. Some examples of passive techniques include modification of the nozzle exit, use of non-axisymmetric nozzle shapes, and the use of tabs or chevrons. Though these techniques have shown several promises, there are demands for alternative techniques to reduce noise more efficiently. In particular, the methods which do not interfere with the primary nozzle flow and which can actively control the jet noise are required.

One of the active methods is the microjet injection at the nozzle exit. We can find several contributions so far in this technique which show positive effects of microjet.

In the present study, a high aspect-ratio rectangular nozzle was adopted as the jet nozzle. It was expected that the combination of non-circular nozzle and microjet injection could be very effective for supersonic jet noise reduction based on the literature knowledge of low noise characteristics of non-circular nozzles. It is also expected that the flow field would be 2D-like and flow mechanism of noise reduction might be easily detected. The nozzle was equipped with forty-four evenly spaced micro-nozzles at the long sides of the nozzle exit. The acoustic measurements were conducted in the far field around the jet, and the flow field visualization with schlieren technique was also conducted in order to obtain an understanding of the noise reduction mechanism by microjet injection.

3.1 Experimental Method

An anechoic chamber was used for the experiment. It is driven by a high-pressure air compressor which supplies air at a maximum storage pressure of 0.83MPa. The storage tank has a total capacity of $60m^3$. After leaving from the storage tank, the air is divided into two ducts for the main jet and the microjet. The total pressure of the main jet and the microjet can be controlled independently.

Figure 12 presents the configuration of the jet nozzle with microjet injection holes. A convergent-divergent nozzle with throat height of 6mm was used. The nozzle exit has a rectangular shape with a width of 72mm and a height of 7.4mm. In the case without microjet injection, almost two-dimensional phenomena are expected so that the microjet effects on the flow field can be clearly grasped. The microjets divided at the manifolds are introduced through convergent micro-nozzles which had diameter of 0.8mm at the nozzle exit as shown in Fig.13. The number of the microjet nozzles is 44, which are evenly spaced at both the upper and the lower nozzle lips. By changing the nozzle lip part, hatched in Fig.12 a), the injection angles and positions of injection holes can be changed.

Several types of injection methods were investigated. In the present paper, three of them are introduced, namely, 60deg injection, 90deg injection from 1mm

upstream position, and 90deg injection from 23mm upstream position as shown in Fig.13 a). Here, '1mm' means the distance from the nozzle exit to the injection hole. The 23mm upstream injection hole is located at the upstream end of the nozzle lip parts. The number of the microjet holes was widely changed. In Fig.13 b), active microjet injection holes (indicated with white circles) are shown in the cases of 'all-hole' injection, 'every-three-hole' injection and 'every-six-hole' injection. The corresponding number of microjets was 44 in all-hole injection, 14 in every-three-hole injection, and 6 in every-six-hole injection, respectively.

With a Brüel & Kjær microphone system, the sound pressure and spectrum of jet noise were measured in the far field. As shown in Fig.14, the microphones were positioned on the 1/6 spherical surface of a radius of 0.75m. The angle θ represents the elevation angle, while the angle ϕ represents the azimuthal angle. The measurement ranges of angles ϕ and θ were from 0 to 120 degrees and 0 to 90 degrees, respectively. The measurements were not conducted where microphones were located in the main flow, that is, when both ϕ and θ were smaller than 30 degrees.

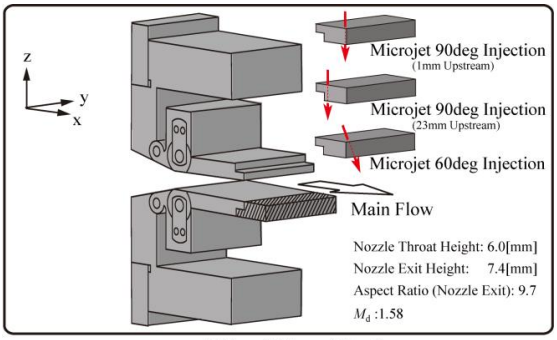

(a) Overall View of Nozzle

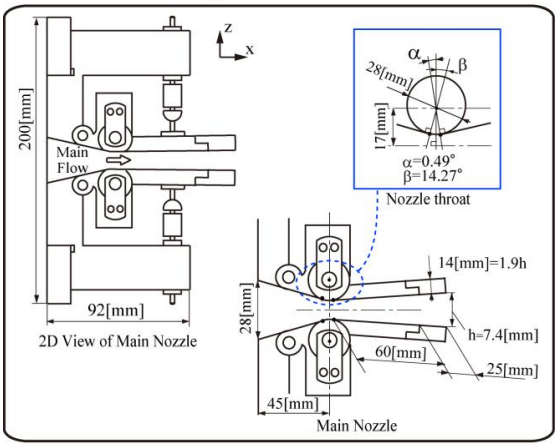

(b) Configuration of 2-D Nozzle

Fig.12 Schematic of nozzle with microjet injection holes

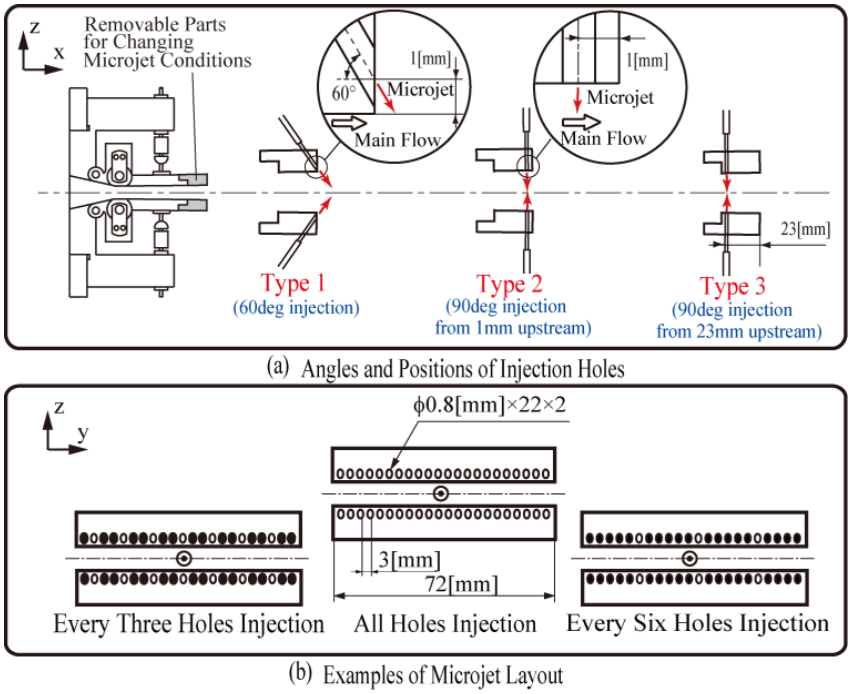

Fig.13 Schematic of micro-nozzle

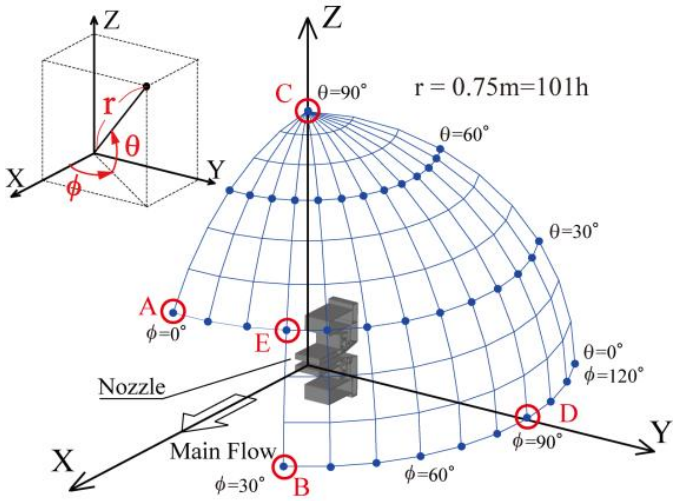

Fig.14 Coordinate system and measurement points

3.2 Results and Discussions

Figure 15 presents the power spectra of the sound pressure in the case of type 2 every-three-hole injection. In the figure, spectra of the cases with microjet pressure of P_m=0.51MPa and P_m=0.20MPa, and the case without microjet are compared. The microphone is located at (θ, ϕ)=(30deg, 0deg), which is right above the main jet.

In the case without microjet, the spectrum peak of the screech tone noise can be seen at the frequency of 7.8 kHz. The peak noise at the frequency from 3 kHz to 5 kHz is composed of the noise from large-scale turbulence and the broadband shock-associated noise, judging from the literature knowledge [8] and configuration of the spectrum. In Fig.15, the broadband noise from 1 to 5 kHz is considerably reduced in the case of P_m=0.51MPa. The screech tone noise is also found to disappear perfectly. In the case of P_m=0.20MPa, however, the reduction of broadband noise is less than the case of P_m=0.51MPa and the screech tone noise is not so much reduced. The mass flux ratio of the microjet to the main jet, Ψ, was 1.05% in the case of P_m=0.51MPa, and 0.24% in the case of P_m=0.20MPa.

In the acoustic measurement, the reduction of the OASPL up to approximately 10dB was observed. In this case, the mass flux ratio of the microjet to main jet was about 1%.

Figure 16 shows the schlieren pictures in the case of M=1.47. The main jet contains shock wave structure. It is clearly seen that large fluctuations of jet shear layers in the case without microjet are suppressed by microjet injection. The large-scale coherent turbulence structures, observed in Fig.16 (a), are also suppressed by microjet. Tam [8] stated that broadband shock-associated noise and screech tone noise are generated only when a quasi-periodic shock cell structure is present in the jet plume. The flow field of the case with microjet loses the periodic shock cell structure. Moreover, the large-scale turbulence structures obviously disappear, as stated above. Therefore, it can be concluded that the interaction between the shock cell and the large-scale turbulence structure could be weakened by microjet and the generation of the shock-associated noise and the screech tone noise could be reduced.

3.3 Concluding Remarks

The effect of microjet injection on supersonic jet noise was found to be remarkable. The broadband peak noise and screech tone noise were greatly reduced using microjet injection. The high frequency turbulent mixing noise was, however, increased due to microjet injection in the sideline and backward direction of the main jet. The unsteady flow field visualization showed that microjet suppressed large fluctuation of jet shear layers, the development of large-scale turbulence structures and the generation of the screech tone noise.

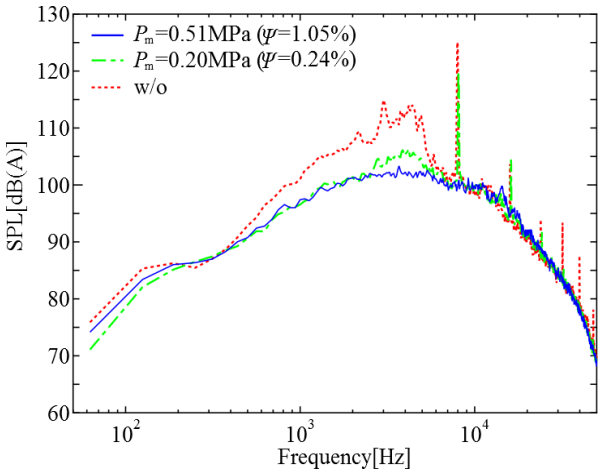

Fig. 15 Example of Power spectra at θ=30deg, ϕ=0deg
(M=1.47, type 2 every three holes injection)

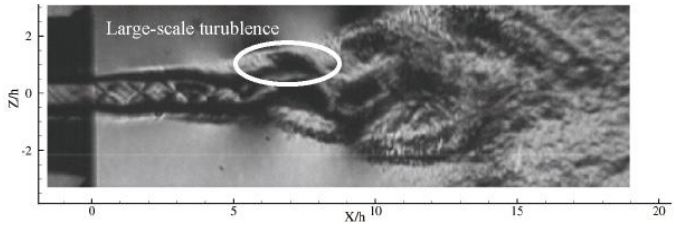

(a) w/o microjet

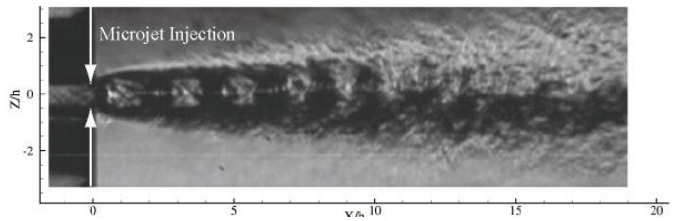

(b) type 2 every three holes injection

Fig. 16 Instantaneous schlieren pictures (M=1.47)

4. Conclusions

Two examples of active control on unsteady flow phenomena were reviewed.

Active suppression of cascade flutter with piezoelectric device was examined by numerical and experimental studies. For transonic compressor cascade in which the shock behavior governed the vibration instability, the control method of active oscillation on blade trailing edge was found to effectively suppress the cascade flutter in the numerical analysis. The potential of the control method was qualitatively revealed in the trial experiment in a transonic cascade tunnel.

For reduction of supersonic jet noise, the microjet injection technique was experimentally investigated in an anechoic chamber. The noise level was effectively reduced up to 10 dB in a point-wise SPL. The flow visualization showed that the unstable motion of supersonic jet with shock structure was dramatically suppressed. The suppression effect probably alleviated the generation of screech tone noise and shock-associated noise.

Though there would be many steps to install these active control methods into aeroengines, the results would provide useful tools for environmentally friendly, ultra-highly efficient engines in the near future.

References

(1) Kazawa, J. and Watanabe, T., “Active Suppression of Cascade Flutter with Piezoelectric Device”, ASME GT2006-90645, Proceedings of ASME Turbo Expo 2006, Barcelona, 2006.

(2) e.g. Vijaya, M. S., “Piezoelectric Materials and Devices”, CRC Press, 2012.

(3) Watanabe, T., Kazawa, J., Uzawa, S., and Keim, B., “Numerical and Experimental Study of Active Flutter Suppression with Piezoelectric Device for Transonic Cascade”, ASME GT2008-51467, Proceedings of ASME Turbo Expo 2008, Berlin, 2008.

(4) Okada, R., Watanabe, T., Uzawa, S., Himeno, T., and Oishi, T., “Investigation of Microjet Injection for Reduction of Supersonic Jet Noise”, ASME GT 2010-23036, Proceedings of ASME Turbo Expo 2010, Glasgow, 2010.

(5) Okada, R., Watanabe, T., Uzawa, S., Himeno, T., and Oishi, T., “ Influence of Microjet Condition on Characteristics of Supersonic Jet Noise and Flow Field, ASME GT 2012-68821, Proceedings of ASME Turbo Expo 2012, Copenhagen, 2012.

(6) NASA “Experimental Quiet Engine Program,” contract No.NAS3-12430, March 1970.

(7) Shibata, T., and Kaji, S., “Role of Shock Structures in Transonic Fan Rotor Flutter,” Unsteady Aerodynamics and Aeroelasticity of Turbomachines, Fransson, T. H. ed., Kluwer Academic Publishers, 1998, pp.733-747.

(8) Tam, C. K. W. “Supersonic Jet Noise”, Journal of Fluid Mechanics, vol.27, 1995, pp17-43.